Effect of particle size distribution on strength of precipitation-hardened alloys

A.J. Kulkarni and K. Krishnamurthy
Department of Mechanical and Aerospace Engineering and Engineering Mechanics, University of Missouri–Rolla, Rolla, Missouri 65409

S.P. Deshmukh and R.S. Mishra[a)]
Department of Metallurgical Engineering, University of Missouri–Rolla, Rolla, Missouri 65409

(Received 29 December 2003; accepted 29 June 2004)

Aging of precipitation hardened alloys results in particle coarsening, which in turn affects the strength. In this study, the effect of particle size distribution on the strength of precipitation-hardened alloys was considered. To better represent real alloys, the particle radii were distributed using the Wagner and Lifshitz and Slyozov (WLS) particle size distribution theory. The dislocation motion was simulated for a range of mean radii and the critical resolved shear stress (CRSS) was calculated in each case. Results were also obtained by simulating the dislocation motion through the same system but with the glide plane populated by equal strength particles, which represent mean radii for each of the aging times. The CRSS value with the WLS particle distribution tends to decrease for lower radii than it does for the mean radius approach. The general trend of the simulation results compares well with the analytical values obtained using the equation for particle shearing and the Orowan equation.

I. INTRODUCTION

Precipitation hardening is a widely used method for increasing the critical resolved shear stress (CRSS) of a material. The CRSS is defined as the resolved shear stress necessary to make dislocations glide over macroscopic distances.[1] In a real material, the motion of a dislocation is affected by precipitates (precipitation hardening) and by atoms dissolved in the matrix (solution hardening). Therefore, in precipitation-hardened materials, the CRSS is defined as the external stress required to overcome the interaction between dislocations and particles.

Particles act as obstacles to the glide of the dislocations and thus reduce their mobility. Dislocations can overcome these obstacles either by shearing these particles or bypassing them. The path a dislocation takes is predominantly dictated by the nature of particles (shearable or unshearable), particle size distribution and the inter-particle spacing.

Aging of precipitation hardened alloys leads to particle coarsening. Coarsening of particles from a very small size at a constant volume fraction helps in increasing the stress required to shear them. However, at a certain radius, it becomes easier for the dislocation to bow around the particles rather than shear them. Beyond this radius, the growth of the particles actually leads to a decrease in the stress required to overcome them, an effect of increased inter-particle spacing.

Existing models for aging response of alloys and the aforementioned two mechanisms predict the CRSS of the material to a modest approximation. These models have been modified and refined according to experimental results obtained for a wide range of materials. But a good estimate of the material strength cannot be obtained because of the inherent simplifications in the model. An alternate approach to obtain the value of CRSS is by simulating the motion of dislocations through an array of obstacles in the microstructure of the material. In a broader context, a computer simulation of the motion of dislocations through a planar random array of obstacles can lead to a better understanding of the influence of microscopic phenomena on macroscopic properties.[1] This understanding can be used in the optimal design of microstructures supporting the vision of "materials by design."[2,3]

Dislocation simulation has been attempted since 1966. Table I[4–17] summarizes the efforts made by researchers in simulation of dislocation-particle interaction. The impetus was given by Foreman and Makin,[5,6] who studied the detailed movement of a dislocation line through a random array of obstacles using a digital computer. Using a point obstacle approximation, justified by the

[a)]Address all correspondence to this author.
e-mail: rsmishra@umr.edu
DOI: 10.1557/JMR.2004.0364

TABLE I. Summary of previous dislocation-particle simulation studies.

Investigators	Suppositions	Results
Kocks[4]	1. Statistical theory 2. Random point-like obstacles	1. Influence of randomness on flow stress 2. Rate of dislocation storage
Foreman and Makin[5,6]	1. Constant line tension 2. Point obstacle approximation 3. Random array of obstacles 4. Dynamics effects neglected 5. Temperature dependent critical breaking angle 6. Circle Rolling Technique	1. CRSS for equal strength particles 2. CRSS for two different strength particles 3. CRSS for spectrum of particle strengths 4. Temperature dependent CRSS
Morris et al.[7–9]	1. Constant line tension 2. Point obstacle approximation 3. Random array of obstacles 4. Dynamics effects neglected 5. Thermally activated glide 6. Circle Rolling Technique	1. Stress for athermal glide 2. Glide path of the dislocation 3. Velocity of glide 4. Temperature dependence of velocity 5. Limiting configuration of obstacles 6. Distribution of forces in limiting configuration 7. Mean dislocation segment length in limiting configuration
Schwarz and Labusch[10]	1. Dislocation Dynamics 2. Solution hardening 3. Random array of obstacles 4. Shearable one-dimensional obstacles 5. Inertia and viscous forces included 6. Thermal activation disregarded 7. Low volume fraction	1. CRSS in absence of inertia effect 2. CRSS in presence of inertia effect 3. Temperature dependent flow stress
Ronnpagel et al.[11]	1. Dislocation dynamics 2. Thermal activation 3. Flexibility of dislocations 4. Three-dimensional obstacles	1. Waiting time at each obstacle 2. Jerky glide of dislocation segments 3. Stress dependence of free activation enthalpy and stress independence of attack frequency 4. Localization of activation
Zhu and Starke, Jr[12]	1. Constant line tension 2. Unshearable particles 3. Spherical/linear particles 4. Random array of particles 5. Dynamics effects neglected 6. Circle Rolling Technique	1. Modified version the Orowan equation 2. Decreasing dependence of CRSS on obstacle size 3. CRSS with linear obstacles
Zhu et al.[13]	1. Constant line tension 2. Shearable/Unshearable particles 3. Spherical/linear particles 4. Superposition/bimodal distribution 5. Random array of particles 6. Dynamics effects neglected 7. Circle Rolling Technique	1. CRSS due to mixture of unshearable point-like particles and shearable point-like particles 2. CRSS due to mixtures of two types of unshearable particles 3. Exponents of Superposition law calculated
Mohles et al.[14,15,16]	1. Dislocation dynamics 2. Viscous drag effects 3. Elastic self-interaction of the dislocation 4. Inertia effect neglected 5. Obstacle distribution through TEM images 6. Shearable/Unshearable 7. Average particle size 8. Ostwald ripening of particles	1. Incorporation of particle coarsening 2. CRSS for each average particle radius 3. Practical obstacle fields 4. Configurations for under-aged, peak-aged and over-aged states 5. CRSS using edge and screw dislocation for range of radii 6. Randomness parameter
Takahashi et al.[17]	1. Multi-scale simulation 2. Molecular dynamics modeling 3. Dislocation dynamics simulation	1. Interaction between γ' phase and dislocation 2. Bow out angle using molecular dynamics 3. Resistance of particle 4. Configurations of dislocations using dislocation dynamics simulation

short-range interaction between the obstacle and the dislocation line, they simulated the motion of a single dislocation line through a random array of obstacles. The critical angle between the arms of the dislocation corresponding to each obstacle was used as the breakaway criterion. Zhu et al.[12,13] studied the strengthening effects due to unshearable spherical, rodlike, and platelike obstacles. In their simulation they introduced the η criterion to determine the instability of the dislocation configuration in terms of the spacing η of any two face-to-face bowed-out dislocation segments. Mohles et al.[14–16] simulated dislocation glide using the local stress equilibrium

along the dislocation line. They have considered Ostwald ripening[18] of particles. They considered a constant volume fraction and varied the particle radii to obtain under-aged (essentially shearable), over-aged (non-shearable), and peak-aged particles. In their recent work they have simulated Orowan process controlled dislocation glide in particle radii distribution of varying randomness.[16] Their results showed a dependence of the CRSS on the particle volume fraction, the mean particle radius and randomness parameter.

Previous studies such as those stated above have either considered a mean radius or a random distribution approach to populate the particle system. In an effort to simulate a real microstructure, in this work, the effect of the particle size distribution on the strength of precipitation-hardened alloys is studied as a function of aging. Results are obtained for an Al-6Mg–1Sc–1Zr alloy in which the particles are distributed using the Wagner[19] and Lifshitz and Slyozov[20] (WLS) theory. The radii and the number of particles are determined for a range of aging times and used to populate the glide plane. The results are then compared with those obtained by simulating the dislocation motion through the same system but with equal strength particles, which represent mean radii. A comparison is also made with the results obtained by using analytical expressions for stress.

II. POPULATION DENSITY FUNCTION FOR PARTICLES

The effect of precipitate ripening is especially important when aging of alloys is considered. At a particular aging temperature, the particle size increases with aging time. This is significant since the strength of an alloy increases as the particle radius increases, reaches a maximum at peak age condition, and then decreases as it becomes easier for a dislocation to bow around the particles rather than to shear them. To simplify the analysis, the radius of each particle, which increases with aging, in the glide area could be assumed to be the same. But using this approach will result in erroneous strength values because it does not model the actual system. On the other hand, considering a particle size distribution is better because it better represents the actual microstructure of the alloy.

The WLS distribution predicts the coarsening characteristics of particles.[19–21] In this theory, the continuity equation that relates the change of the population density function as the particles grow is given by

$$\frac{\partial F(r,t)}{\partial t} + \frac{\partial}{\partial r}\left[F(r,t)\left(\frac{\partial r}{\partial t}\right)\right] = 0 \quad , \tag{1}$$

where $F(r, t)$ is the population density function, r is the particle radius and t is the aging time. Equation (1) can be rewritten using the normalized time and space parameters defined as

$$\rho = \frac{r}{r_m} \text{ and } \tau = \frac{t}{t_m} \quad , \tag{2}$$

where the suffix m refers to mean states. Using a separation of variables technique, the space solution, which is plotted in Fig.1, for the problem is given by[20]

$$g(\rho) = \frac{4}{9}(\rho)^2\left(\frac{3}{3+\rho}\right)^{\frac{7}{3}}\left(\frac{1.5}{1.5-\rho}\right)^{\frac{11}{3}} \exp\left(\frac{\rho}{\rho-1.5}\right) \quad \text{for } 0 \leqslant \rho < 1.5 \quad , \tag{3}$$

$$g(\rho) = 0 \text{ for } \rho > 1.5 \quad ,$$

and the variation of the solution in time is given by

$$h(\tau) = \frac{3f}{4\pi r_m^4}\left(\frac{1}{\int_0^\infty \rho^3\, g(\rho)d\rho}\right) \quad , \tag{4}$$

where f is the volume fraction and the mean radius is predicted by the kinetic equation, which expresses the growth of mean radius as a function of time given by[22]

$$[r_m(\tau)]^3 - [r_m(0)]^3 = \frac{4}{9}\tau \quad . \tag{5}$$

The population distribution function, $F(\rho, \tau)$, obtained as a product of the time and space domain solutions, is plotted for increasing aging times in Fig. 2. Also, the distribution function $F(r, t)$ is plotted for incremental particle radius by reverting back to the original parameters. Note that with increased aging time, smaller particles dissolve while larger particles grow in size. The distribution function was used to determine the number

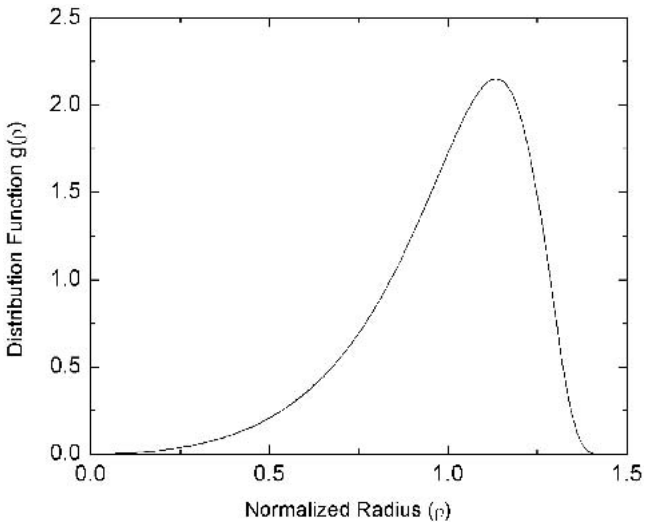

FIG. 1. Distribution function $g(\rho)$ plotted for normalized particle radius ρ.

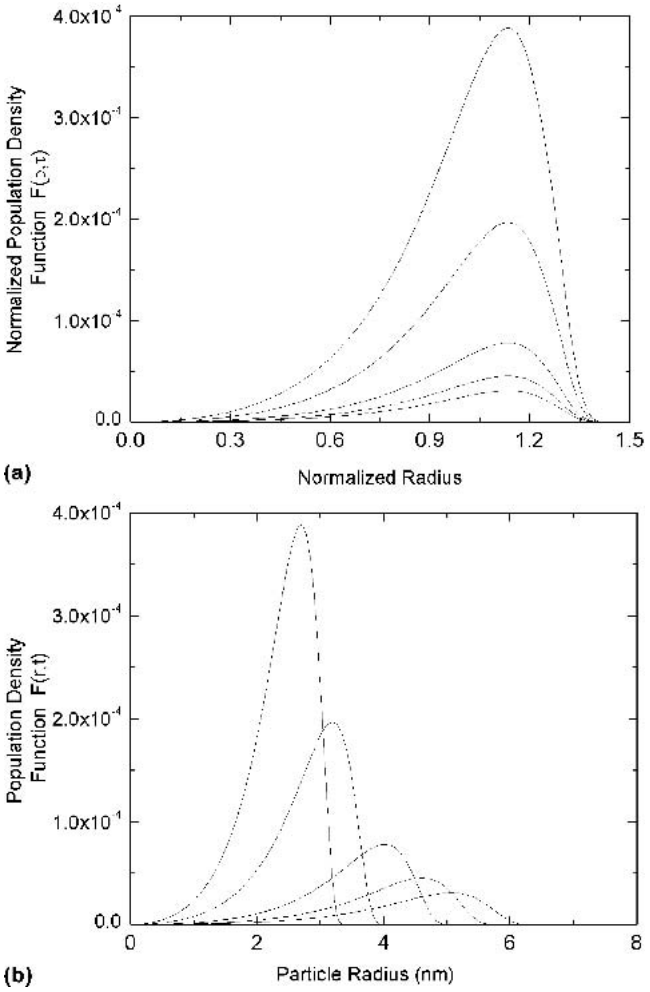

FIG. 2. Plot of Density function: (a) $F(\rho, \tau)$ versus ρ and (b) $F(r, t)$ versus r.

of particles per unit volume N_v for a range of aging times. If the probability of the particle intersecting the glide area is assumed proportional to its radius and all the particles are expected to be intersected at the center, the number of particles per unit glide area can be calculated as[23]

$$N_p = 2rN_v \quad . \tag{6}$$

This distribution can be used only when all the particles are intersected at the center. A better distribution can be obtained by considering the probability of a particle intersecting the glide plane at a radius r which varies from 0 to the particle radius R.[1,24] The probability of obtaining a circle of radius r from a sphere of radius R is equal to the vertical thickness of a slice of the sphere with that radius, i.e., an intercept of radius r can be formed if the center of the particle lies within a distance of $\sqrt{R^2 - r^2}$ from the intersecting plane (Fig. 3). The distribution of the intercepts can be written as[24]

$$\frac{dz}{R} = \frac{rdr}{R\sqrt{R^2 - r^2}} \quad . \tag{7}$$

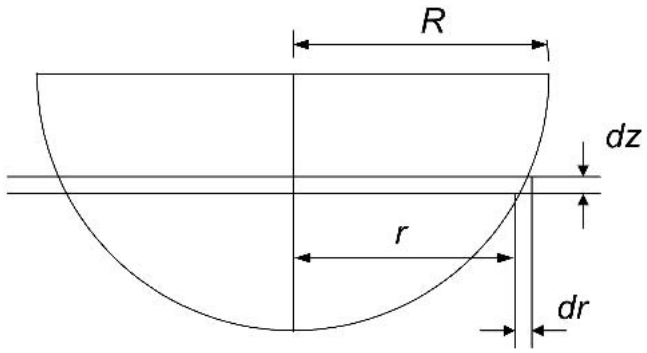

FIG. 3. Intersection of plane with the particle at an arbitrary radius r.

This distribution is expected for each of the particle sizes considered in the WLS distribution. Hence, an intersection of a radius r can be obtained from a range of spheres with radii greater than r. The total number of particles can then be determined by using the distribution in Eq. 6 with the WLS distribution given by Eq. (3). The values of the intersection radii distribution obtained from the WLS distribution (N_I) are plotted for a range of particle radii in Fig. 4. It can be clearly seen that for larger aging times, the need for integer values for the number of particles results in some error in approximating the distribution curve. Figure 4 also shows that as the aging time increases, the radius of particle increases, or precipitate coarsening occurs, and the number of particles decreases because the volume fraction is assumed constant.

III. SIMULATION SCHEME

A. Populating the glide plane

Populating the glide plane consists of determining the particle size distribution, i.e., the size and the number of particles of that size, and specifying the position of the

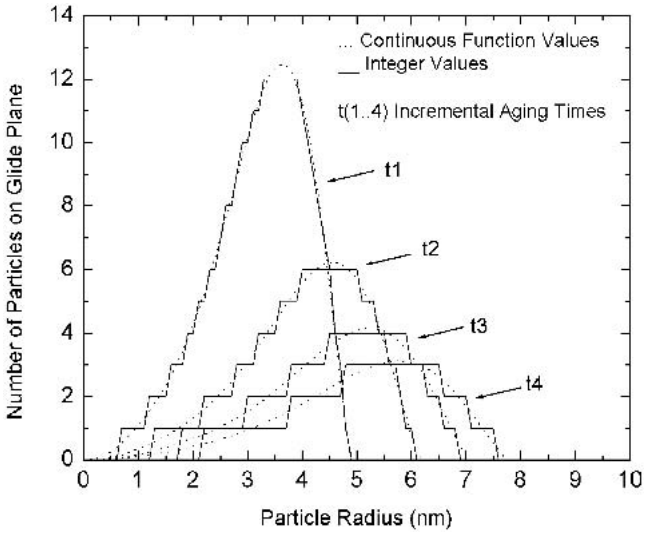

FIG. 4. Change in number of particles with increasing aging time.

particles on the glide plane. For the mean radius case, particles of equal size were randomly distributed in the glide plane. However, for the particle size distribution case, the number of particles of each radius was determined using the WLS distribution. The aging time was varied such that mean particle radius increased from 1 to 17 nm for the example alloy considered in this study.[25] Strength values were assigned to the particles depending on their radius and were defined by the critical angle ϕ_{cr} of the dislocation. For smaller particles or weak obstacles, the critical angles were calculated from the Friedel estimate given by[5,26]

$$\sigma = \frac{Gb}{\lambda}\left(\cos\frac{\phi_{cr}}{2}\right)^{3/2} \quad , \tag{8}$$

where σ is the shear stress, ϕ_{cr} is the critical angle, G is the shear modulus, b is the Burger's vector, and λ is the inter-particle spacing, and the equation for particle shearing given by

$$\sigma_{APB} = (3.1)\frac{\gamma^{3/2}}{b^2}\sqrt{rf/G} \quad , \tag{9}$$

where σ_{APB} is the yield strength, f is the volume fraction, and γ is the energy required to form the APB. The dependence of the radius of particles on inter-particle spacing can be expressed as[23]

$$\lambda = 1.23r\sqrt{\frac{2\pi}{3f}} \quad . \tag{10}$$

Equations (8–10) were used to calculate the critical angle for each radius as

$$\phi_{cr} = 2\cos^{-1}\left(\frac{\sqrt{f}\gamma^{3/2}}{G^{3/2}b^3}(\lambda\sqrt{r})\right)^{2/3} \quad . \tag{11}$$

If the volume fraction is a constant, Eq. (11) can be rewritten as

$$\phi_{cr} = 2\cos^{-1}[K(\lambda\sqrt{r})]^{2/3} \quad , \tag{12}$$

where K is a constant that takes the value,

$$K = \frac{\sqrt{f}\gamma^{3/2}}{G^{3/2}b^3} \quad . \tag{13}$$

Equation (10) clearly shows that the critical angle depends on the radius of the particles. The critical angle values as a function of the radii have been shown in Fig. 5. These values were assigned to each radius used in the simulation. For larger particles or strong obstacles, the critical angle can be calculated to be equal to zero.

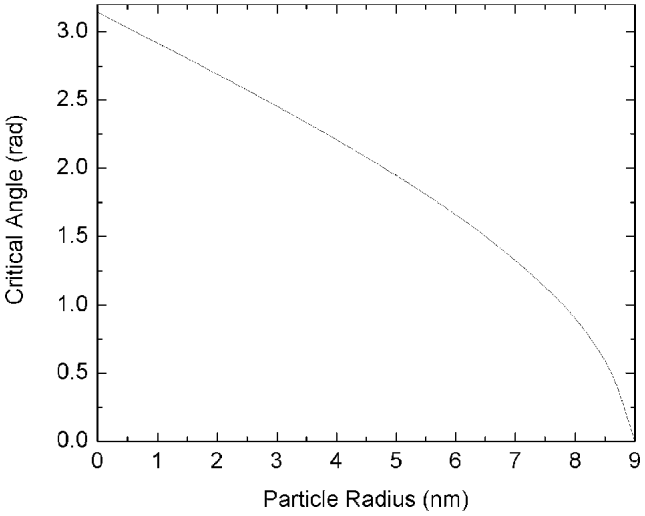

FIG. 5. Variation of critical angle with radius of particles.

B. Dislocation motion

Once the glide plane was populated, the dislocation line was run through the area and the CRSS was calculated from the dislocation-particle interactions. A constant line tension approach was used to depict the interactions. The simulation was started with the dislocation line, initially straight, approaching the particles. Depending on the initial stress, the dislocation bowed out to a stable configuration. Cyclic boundary conditions were imposed on the dislocation during its motion. The stable configuration was defined by the maximum bow-out radius of the dislocation segments. This bow-out radius was calculated as[4,27,28]

$$R = \frac{T}{\sigma_a b} \quad , \tag{14}$$

where σ_a is the applied shear stress, and T is the line tension, which can be written as[27,28]

$$T = \frac{Gb^2}{4\pi}\ln\frac{\lambda}{b} \quad . \tag{15}$$

The applied stress was increased until the obstacle was overcome; the dislocation moved forward in the glide plane and was incident on the next particle. New particles were found by sweeping the glide area by using a circle rolling procedure.[8] The detachment criterion was the included angle between the arms of the dislocation corresponding to each particle. Figure 6 shows the calculation of the included angle for symmetric and asymmetric dislocation configurations.[1] The dislocation line can form symmetrical or asymmetrical configurations depending on the positional variation of the particles. A symmetrical configuration is formed when the inter-particle spacing between the particles is equal and they share the same

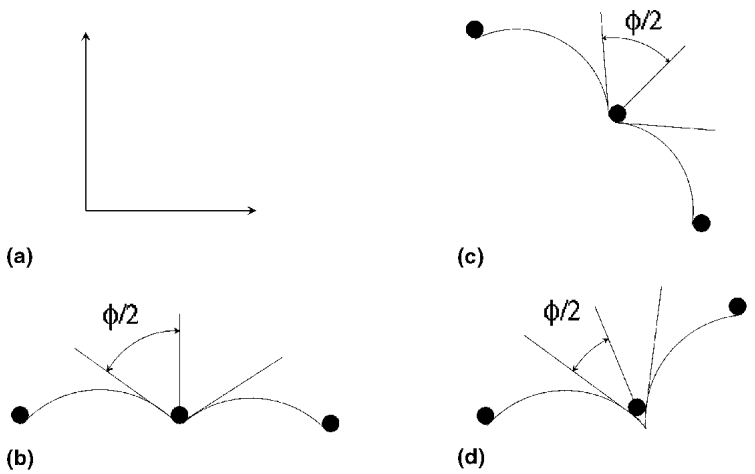

FIG. 6. Calculation of included angle ϕ for different dislocation configurations, (a) coordinate frame, (b) symmetric dislocation configuration, (c) asymmetric dislocation configuration, and (d) asymmetric dislocation configuration.

abscissa, as shown in Fig. 6(b). Asymmetrical configurations are formed due to the random relative positioning of the particles, as shown in Figs. 6(c) and 6(d).

The critical angle for each particle depends upon its radius and was assigned when the glide plane was populated. A smaller value of critical angle essentially depicts a larger particle or stronger obstacle and vice-versa, which determines whether the obstacle will be circumvented or sheared. At each position of the dislocation, the included angle was calculated, compared with the particle critical angle and the dislocation was released when the critical angle was reached. After release, the dislocation moved to the next set of particles and bowed out to the equilibrium radius depending on the applied stress. The simulation was terminated after the dislocation exits the predefined glide area. The maximum value of stress obtained for a specific position of the particles was the CRSS for the material.

A single value for the CRSS is difficult to determine because the population of the glide area is different with each simulation run. The dislocation encounters different particle strength values, inter-particle spacing and orientation of the particles. Therefore, to accurately simulate the motion of the dislocation, the aforementioned effects are included in the model and, a range of values are obtained for the CRSS instead of a single value.

IV. SIMULATED RESULTS

To illustrate the simulation scheme, results are presented for the simulation of dislocation motion for an Al–6Mg–1Sc–1Zr alloy with a volume fraction $f = 0.0274$. In this study, the following material constants were assumed: G = 27 GPa, APB energy $\gamma = 0.185$ J/m^2, and Burgers vector $b = 0.289$ nm.[3,25]

The WLS distribution was used to populate the glide plane such that the mean radii varied from 1 to 17 nm in 1-nm increments. Each case was repeated ten times to study the variability of the CRSS values. Figure 7 shows the mean CRSS value and the spread in each case. The spread shows the maximum and minimum values of CRSS found at each radius. It can be seen from the figure that the spread, although not significantly large, does exist for the system under consideration.

Figures 8–10 show the initial (IC), maximum stress (MSC), and final (FC) configurations of the dislocation line for three representative cases involving mean radius particles. Although the mean radius approach and WLS distribution require the number of particles to decrease with an increase in aging time, the number of particles was maintained constant and the glide area and inter-particle spacing were rescaled appropriately to maintain accuracy of the simulation.

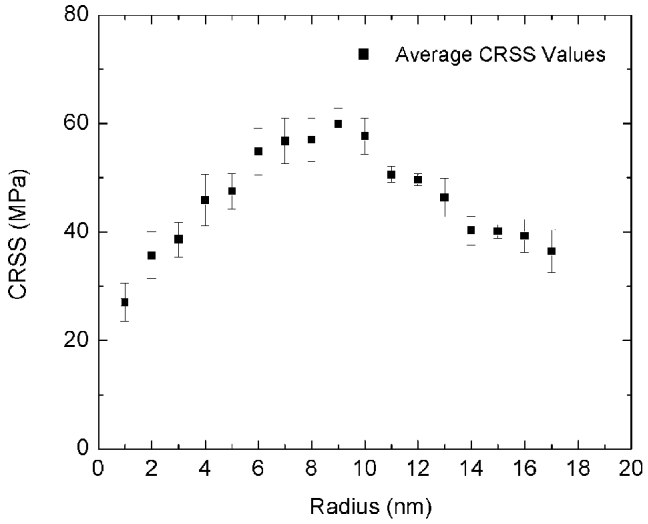

FIG. 7. Mean CRSS values and their spread using the WLS approach.

Figure 8 shows the motion of the dislocation in a particle field of 100 particles with a mean radius of 2 nm corresponding to a low aging time. It can be seen that for small particles, the bow out radius is very large and the dislocation appears almost to be straight. The simulation was stopped at the point when the line exits the predefined glide area. For the system considered, the CRSS was reached approximately halfway through the glide plane and the rest of the simulation shows the dislocation as it moves out of the glide area.

For a higher aging time, the particles were distributed with a mean radius of 5 nm. Figure 9 shows a configuration for that radius. The bow-out radii are smaller than those in the earlier case, and the dislocation line no longer remains straight during its motion. Increasing the aging time further increases the particle radii. Figure 10 shows the dislocation line interacting with the particles with a 9-nm mean radius. With increased radius, the dislocation bow-out radius decreases and the line becomes unstable. In other words, the bow-out radius becomes smaller than the inter-particle spacing, at certain

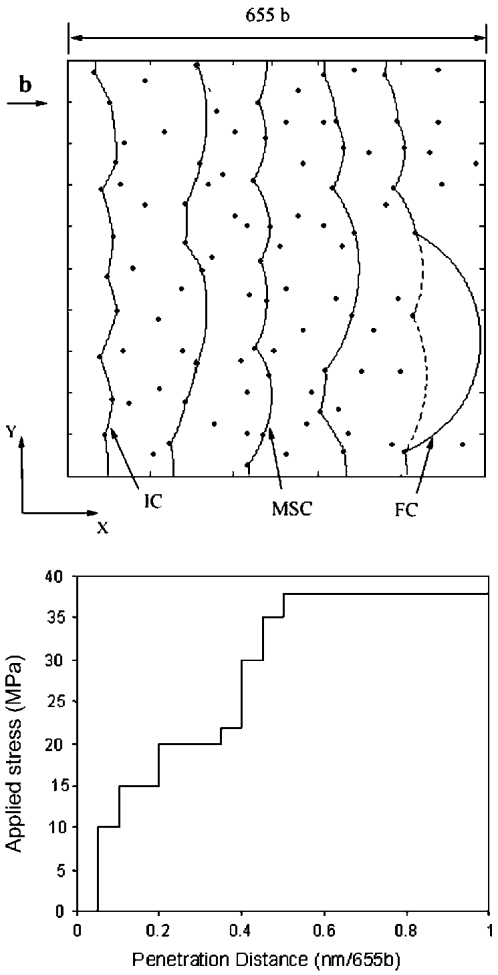

FIG. 8. Movement of dislocations in a glide plane populated with particles with a mean radius of 2 nm.

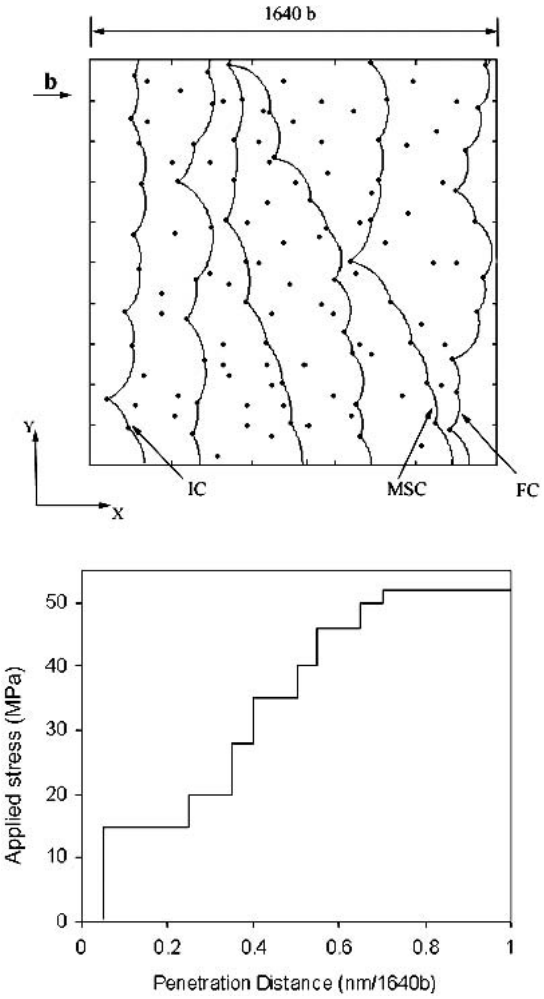

FIG. 9. Movement of dislocations in a glide plane populated with particles with a mean radius of 5 nm.

points in the simulation. For this radius, the dislocation line loops most of the particles in its path. The loops encircling the particles after the dislocation has moved ahead are not displayed.

To study the error introduced by assuming a mean radius, the dislocation motion was simulated with the glide plane populated by particle with radius given by the mean radius. Figure 11 shows a comparison of the CRSS values obtained by assuming particle radii to be distributed by the WLS approach and assuming particles to be of the same size. This figure also shows the analytical values obtained by using the equation for particle shearing and Orowan equation given by

$$\tau_{\mathrm{APB}} = \frac{\gamma^{3/2}}{b^2}\sqrt{rf/G} \quad , \tag{16a}$$

$$\tau_{\mathrm{Orowan}} = (0.84)\,\frac{Gb}{\lambda} \quad . \tag{16b}$$

Figure 11 clearly shows that the CRSS value with the

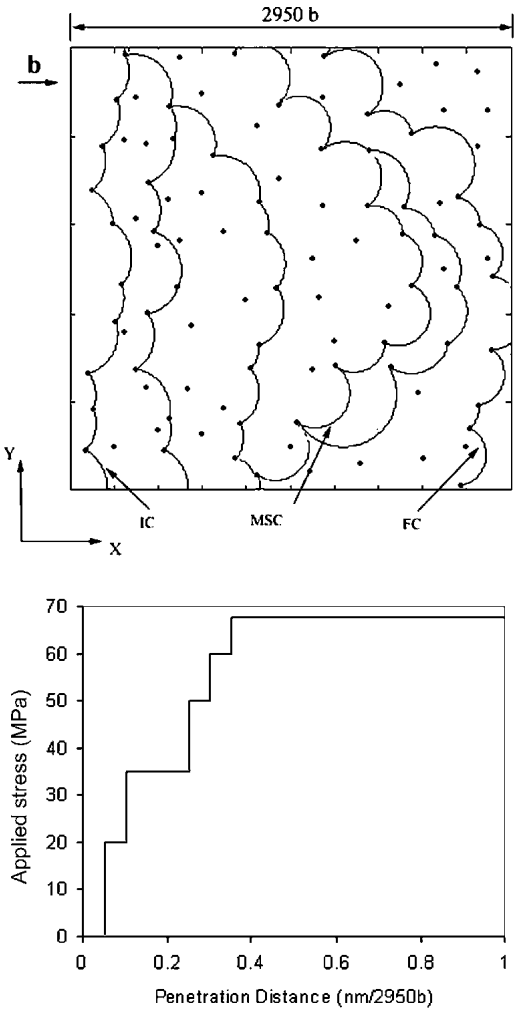

FIG. 10. Movement of dislocations in a glide plane populated with particles with a mean radius of 9 nm.

WLS particle distribution tends to decrease as compared to the mean radius approach. The lower values are due to the distribution effect. With the distribution incorporated in the system, particles smaller than the mean are present in the glide plane. Therefore, when the particles are distributed, which is a more accurate description of real materials, the system weakens. This explains the lower CRSS values with WLS distribution.

Figure 11 also shows that the CRSS values tend to approximate the analytical values in the under-aged state. Moreover, the CRSS values from these two approaches are below those obtained by using Eqs. (16a) and (16b). The simulation approach reduces the impact of the simplification inherent in the analytical models.

V. CONCLUDING REMARKS

In this study, the effect of particle size distribution of the strength of aging alloys was considered. Results obtained show the strength decreasing with the distribution

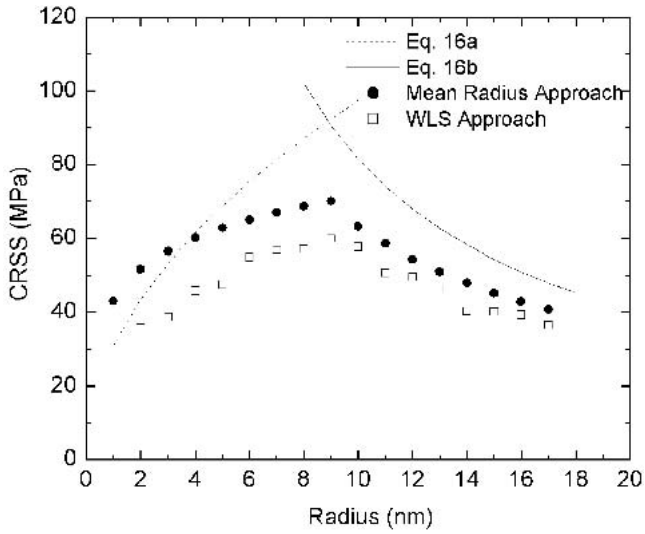

FIG. 11. Comparison of CRSS values obtained from simulation using WLS and mean radius approaches and analytical expressions.

in effect. This study can be extended to represent the real material even more realistically by incorporating microstructure evolution in the simulation. The nucleation and growth of precipitates and its effect on volume fraction can be studied and used in the simulation. The CRSS values obtained by the simulation scheme presented can be used to design materials more efficiently and discover microstructural compositions that are not intuitive.

ACKNOWLEDGMENTS

The authors would like to gratefully acknowledge the support of the National Science Foundation through Grant No. DMR-0100780 and the University of Missouri Research Board.

REFERENCES

1. E. Nembach: *Particle Strengthening of Metals and Alloys,* 1st ed. (John Wiley and Sons, New York, 1996).
2. G.B. Olson: Computational design of hierarchically structured materials, *Science* **277,** 1237 (1997).
3. A.J. Kulkarni, K. Krishnamurthy, S.P. Deshmukh, and R.S. Mishra: Microstructural optimization of alloys using a genetic algorithm. *Mater. Sci. Eng. A* **372,** 213 (2004).
4. U.F. Kocks: A statistical theory of flow stress and work hardening. *Philos. Mag.* **13,** 541 (1962).
5. A.J.E. Foreman and M.J. Makin: Dislocation movement through random array of obstacle, *Philos Mag.* **14,** 911 (1966).
6. A.J.E. Foreman and M.J. Makin: Dislocation movement through random array of obstacle. *Can. J. Phys.* **45,** 511 (1967).
7. J.W. Morris, Jr. and D.H. Klahn: Thermally activated dislocation glide through a random array of point obstacles: computer simulation. *J. Appl. Phys.* **45,** 2027 (1974).
8. J.W. Morris, Jr. and D.H. Klahn: Statistics of the thermally activated glide of a dislocation through a random array of point obstacle. *J. Appl. Phys.* **44,** 4882 (1973).

9. K. Hanson and J.W. Morris, Jr.: Limiting configuration in dislocation glide through a random array of point obstacles. *J. Appl. Phys.* **46,** 983 (1975).
10. R.B. Schwarz and R. Labusch: Dynamic simulation of solution hardening. *J. Appl. Phys.* **49,** 5174 (1978).
11. D. Ronnpagel, Th. Streit, and Th. Pretorius: Including thermal activation in simulation calculation of dislocation glide. *Phys. Status Solidi* **135,** 445 (1993).
12. A.W. Zhu and E.A. Starke, Jr.: Strengthening effect of unshearable particles of finite size: A computer experimental study. *Acta Mater.* **47,** 3263 (1999).
13. A.W. Zhu, A. Csontos, and E.A. Starke, Jr.: Computer experiment on superposition of strengthening effects of different particles. *Acta Mater.* **47,** 1713 (1999).
14. V. Mohles, D. Ronnpagel, and E. Nembach: Simulation of dislocation in precipitation hardened materials. *Comput. Mater. Sci.* **16,** 144 (1999).
15. V. Mohles and E. Nembach: The peak and overaged states of particle strengthened materials: Computer simulations. *Acta Mater.* **49,** 2405 (2001).
16. V. Mohles and B. Fruhstorfer: Computer simulation of orowan process controlled dislocation glide in particle arrangement of various randomness. *Acta Mater.* **50,** 2503 (2002).
17. A. Takahashi, N. Soneda, and G. Yagawa: In *Material Modeling-Atomistic Level,* edited by H.A. Mang, F.G. Rammerstorfer, and J. Eberhardsteiner (Fifth World Congress on Computational Mechanics, Vienna, Austria, 2002).
18. W. Ostwald: Periodische Erscheinungen bei der auflosung des chroms in sauren. *Zeistschr. Phys. Chem.* **34,** 495 (1900).
19. C. Wagner: Theorie der Alterung von Niederschlagen durch Umlosen (Ostwald-Reifung). *Z. Elektrochem.* **65,** 581 (1961).
20. I.M. Lifshitz and V.V. Slyozov: The kinetics of precipitation from supersaturated solid solutions. *J. Phys. Chem. Solids* **19,** 35 (1961).
21. L. Ratke and P.W. Voorhees: *Growth and Coarsening: Ostwald Ripening in Material Processing,* 1st ed. (Springer-Verlag, Berlin, Germany, 2002).
22. D. Porter and K. Easterling: *Phase Transformations in Metals and Alloys,* 1st ed. (T.J. Press (Padstow) Ltd., Cornwall, U.K., 1981).
23. J.W. Martin: *Precipitation Hardening,* 1st ed. (Pergamom Press Ltd., Oxford, U.K., 1968).
24. J.C. Russ and R.T. Dehoff: *Practical Stereology*, 2nd ed. (Kluwer Academic/Plenum Publishers, New York, 2000).
25. K.L. Kendig and D.B. Miracle: Strengthening Mechanisms of an Al-Mg-Sc-Zr Alloy, *Acta Mater.* **50,** 4165 (2002).
26. J. Friedel, *Dislocations,* 1st ed. (Addison-Wesley, Reading, Massachusetts, 1964).
27. J.P. Hirth and J. Lothe: *Theory of Dislocations,* 2nd ed. (John Wiley and Sons, New York, 1982).
28. F.R.N. Nabarro: *Theory of Crystal Dislocations* (Oxford University Press, London, U.K., 1967).